6-2023

An Examination of the Stiffness Terms Needed to Model the Dynamics of an Eddy Current based Maglev Vehicle

Colton W. Bruce
Portland State University, bcolton@pdx.edu

Jonathan Bird
Portland State University, bird@pdx.edu

An Examination of the Stiffness Terms Needed to Model the Dynamics of an Eddy Current based Maglev Vehicle

Colton Bruce, Jonathan Z. Bird

Laboratory for Magnetomechanical Energy Conversion and Control
Portland State University, Department of Electrical and Computer Engineering, Portland, OR, USA, bird@pdx.edu

This paper re-examines the basis for each eddy current stiffness term computed from prior published steady-state eddy current models. The paper corrects prior analysis work by confirming, through the use of 2-D and 3-D dynamic finite element analysis modelling, that when a magnetic source is moving over an infinite-wide and infinite-long conductive sheet guideway the steady-state lateral and translational stiffness terms will be zero and only the vertical coupled stiffness terms need to be modelled. Using these observations, a much simplified 6 degrees-of-freedom (DoF) linearized eddy current dynamic force model can be used to compute the steady-state force changes in eddy current based maglev vehicles when operating over a wide uniform conductive track.

Index Terms— Eddy current, electrodynamic wheel, lift-to-drag ratio, maglev, magnetic levitation, stiffness.

I. INTRODUCTION

THE rotation of a permanent magnet rotor above a conductive, non-magnetic, flat track induces large eddy currents in the track that creates an opposing lift and thrust force. Both radial [1-4] and axial [4, 5] rotor configurations have recently been studied. An example of a one pole-pair radial rotor, also called an electrodynamic wheel (EDW), is illustrated in Fig. 1. Magnetic levitation (maglev) vehicles using a six wheeled [1] and four wheeled [2-4] radial EDWs have recently been tested. The EDW–Maglev allows the track to be fully passive which greatly lowers the cost of the maglev infrastructure, and the vehicle can be constructed using relatively low-cost components.

To provide good vehicle control the EDW forces as a function of position (stiffness) and velocity (damping) need to be accurately modelled and controlled. The lift, thrust and lateral forces are highly coupled and depend on the angular speed ω, velocity (v_x, v_y, v_z) and airgap height y_g. The computation of the forces as a function of these variables using a numerical approach, such as 3-D time changing finite element analysis (FEA), is computationally expensive. It is challenging to numerically model both the simultaneous high-speed rotation and translation velocity along a long finite-thickness conductive track. For this reason, 3-D analytic based steady-state modelling methods have been developed [3, 6-8].

The use of the second-order vector potential (SOVP) analytic method has been shown to be effective at simplifying the number of unknowns to solve for in certain 3-D eddy current problems. For instance, Theodoulidis and Bowler pioneered the use of the SOVP method to compute the field distribution in a right-angle conductive wedge [9]. Musolino *et al.* used a cylindrical SOVP formulation to study the currents induced by moving coils over a tubular conductive cylinder [10]. And Chen *et al.* [11] and Paul *et al.* [3, 6-8] have utilized the Cartesian SOVP formulation to compute the forces created by translating and rotating magnets over a finite thickness conductive plate. When the conductive plate is thin and very wide, then the field decays before reaching the edges of the plate, in such cases, the

SOVP unknowns can be reduced to only one, further reducing the modeling complexity [6, 7].

Prior papers have used analytic-based fictitious magnetic charge methods to compute the force and derive stiffness and damping terms for an EDW [3, 8]. However, these prior papers incorrectly indicated that certain lateral and translational stiffness terms are non-zero for infinitely wide and long tracks. The purpose of this paper is to correct this misinterpretation and confirm through the analytic force formulation and FEA computational analysis that when the track edge-effects can be neglected then the lateral and translational stiffness terms are zero. Consequently, the 3-D stiffness equations needed to model the dynamics of a 6-degree-of-freedom (6-DoF) EDW–Maglev are greatly simplified.

II. FORCE AND ENERGY

The derivation of the magnetostatic force from the system energy can be completed by using the same approach as for electrostatic charges [12, 13]. For example, the fields emanating from two diametrically magnetized cylinder magnets can be accurately modelled by utilizing a fictious magnetic charge distribution whose magnitude varies sinusoidally [14]. A 2-D sketch of two charge sheet cylinders is illustrated in Fig 2(a). The sinusoidal distributed surface magnetic charge distribution functions are ρ_s, and ρ_r. Assume that the charge functions ρ_s and ρ_r are immutable, and therefore the self-energy of the charge dis-
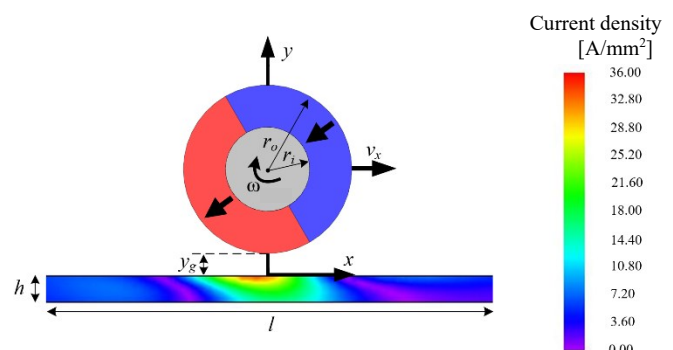

Fig. 1. A single $P = 1$ pole-pair radial EDW, the induced current density in the conductive track along with the geometric definitions are also shown.

tribution will not change. The total mutual energy U between the charge distributions is then [12]

$$U = \int_V [\rho_r \phi_s + \rho_s \phi_r] dv \tag{1}$$

where ϕ_s and ϕ_r are the respective scalar potential fields created by the top and bottom magnetic charge cylinder distributions. The integral is evaluated around a sufficiently large volume region such that at the volume edges the field approaches zero. A mechanical energy W keeps the charge cylinders in place. Given the principle of conservation of energy, the following is true

$$\frac{d}{dt}(U + W) = 0 \tag{2}$$

or

$$dU + dW = 0 \tag{3}$$

Now suppose that the charge distribution ρ_r undergoes a small virtual displacement $d\mathbf{l}$, due to a magnetostatic force $\mathbf{F}$. Due to the virtual displacement, the magnetostatic field's mutual energy between the charge distributions must change. The change in magnetostatic mutual energy, due to the change in position, can be expressed as

$$dU = \nabla U \cdot d\mathbf{l}\big|_{\rho_s, \rho_r = constant}. \tag{4}$$

This incremental change in mechanical energy is then equal to the work done by the force

$$dW = \mathbf{F} \cdot d\mathbf{l}. \tag{5}$$

Combining (3) and (5) gives

$$\mathbf{F} \cdot d\mathbf{l} = -dU\big|_{\rho_s, \rho_r = constant}. \tag{6}$$

and substituting (4) into (6) gives

$$\mathbf{F} \cdot d\mathbf{l} = -\nabla U \cdot d\mathbf{l}\big|_{\rho_s, \rho_r = constant}. \tag{7}$$

Since the relationship is independent of the direction of $d\mathbf{l}$, it can be concluded that

$$\mathbf{F} = -\nabla U\big|_{\rho_s, \rho_r = constant}. \tag{8}$$

In Cartesian coordinates the incremental change vector and force vectors can be described by

$$d\mathbf{l} = \delta_x \hat{\mathbf{x}} + \delta_y \hat{\mathbf{y}} + \delta_z \hat{\mathbf{z}} \tag{9}$$

$$\mathbf{F} = F_x \hat{\mathbf{x}} + F_y \hat{\mathbf{y}} + F_z \hat{\mathbf{z}} \tag{10}$$

where the circumflex denotes unit vectors. The force between the two magnets can be computed by evaluating across a surface between the magnets such that [12]

$$\mathbf{F} = -\frac{1}{\mu_o} \int_{-l/2}^{l/2} \int_{w/2}^{w/2} \rho_s \nabla \phi_r \, dz dx \bigg|_{\rho_s, \rho_r = constant} \tag{11}$$

where the integrals are evalated over a length l and width w that is sufficiently long and wide that the fields are assumed to be zero at the edges. Since [12]

$$\mathbf{B}_r = -\mu_o \nabla \phi_r \tag{12}$$

where

$$\mathbf{B}_r = B_x \hat{\mathbf{x}} + B_y \hat{\mathbf{y}} + B_z \hat{\mathbf{z}} \tag{13}$$

Substituting (12) into (11), the force can be evaluated using [13]

$$\mathbf{F} = \int_{-l/2}^{l/2} \int_{w/2}^{w/2} \rho_s \mathbf{B}_r \, dz dx \bigg|_{\rho_s, \rho_r = constant}. \tag{14}$$
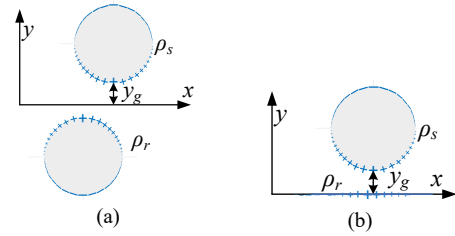

Fig. 2. (a) Sketch of two diametrically magnetized cylinder magnets that are approximated by magnetic charge functions, ρ_r and ρ_s. (b) shows a top source charge function, ρ_s and a bottom charge sheet distributed function, $\rho_r(x,z)$, located at $y=0$ axis. The bottom charge distribution is defined so that it creates an equivalent field representation of the induced eddy currents.

As both charge functions are assumed to not change the stiffness matrix defined as

$$[\bar{\mathbf{k}}] = \begin{bmatrix} k_{xx} & k_{xy} & k_{xz} \\ k_{yx} & k_{yy} & k_{yz} \\ k_{zx} & k_{zy} & k_{zz} \end{bmatrix} = - \begin{bmatrix} \partial F_x / \partial x & \partial F_x / \partial y & \partial F_x / \partial z \\ \partial F_y / \partial x & \partial F_y / \partial y & \partial F_y / \partial z \\ \partial F_z / \partial x & \partial F_z / \partial y & \partial F_z / \partial z \end{bmatrix} \tag{15}$$

can be evaluated directly between the magnets. For example, the first three stiffness terms can be evaluated by computing:

$$[k_{xx}, k_{xy}, k_{xz}] = - \int_{-l/2}^{l/2} \int_{w/2}^{w/2} \rho_s \nabla B_x \, dz dx \bigg|_{\rho_s, \rho_r = constant} \tag{16}$$

Consider now the case in which this force and stiffness evaluation method is extended to the evaluation of steady-state eddy current forces created through the induction of eddy currents in a conductive sheets [3, 6-8]. For example, consider the case shown in Fig 2(b), in which the bottom source field is now a flat magnetic charge sheet. This flat charge sheet can be used to reproduce the reflected field created by a circulated steady-state eddy current distribution. The eddy currents induced by the angular rotation ω and velocity (v_x, v_y, v_z) of the top source field relative to the stationary track. The electrical angular rotational can be modeled in steady-state by using complex functions. The 3-D steady-state eddy current forces for this system has been shown to be accurately computed by [6]

$$\mathbf{F} = \frac{1}{2} \text{Re} \left\{ \int_{-l/2}^{l/2} \int_{w/2}^{w/2} \rho_s^* \mathbf{B}_r \, dz dx \right\} \bigg|_{\rho_s = constant}. \tag{17}$$

where the star superscript denotes conjugation and unlike when using real terms [13] the magnetic charge force equation contains a half term due to the presence of the complex functions [6]. In this case the source field created by ρ_s is immutable, but the eddy current reflected field $\mathbf{B}_r$ must be dependent on ρ_s and not independent of it, like in the case when the two field sources are both from magnets. As a consequence of the reflected field's self-energy is not source independendent. The value of the source field will change with the virtual displacement $d\mathbf{l}$ and therefore the stiffness terms cannot be evaluated using the method shown in (16) because of the dependence of $\mathbf{B}_r$ on ρ_s. As such, the partial derivative of the full force equation, must be evaluated. All terms in the force equation, (17), then need to be evaluated and the gradient cannot be evaluated only on the individual $\mathbf{B}_r$ terms. For the case of the EDW the steady-state force component terms were previously derived and they are [6]

$$F_{x,s} = \frac{wl}{\mu_0} \text{Re} \left\{ \sum_{m=-M}^{M} \sum_{n=-N}^{N} \left| S_{mn}^y \right|^2 e^{-2\kappa_{mn} y_g} j \frac{\xi_m}{\kappa_{mn}} R_{mn} \right\} \quad (18)$$

$$F_{y,s} = -\frac{wl}{\mu_0} \text{Re} \left\{ \sum_{m=-M}^{M} \sum_{n=-N}^{N} \left| S_{mn}^y \right|^2 e^{-2\kappa_{mn} y_g} R_{mn} \right\} \quad (19)$$

$$F_{z,s} = \frac{wl}{\mu_0} \text{Re} \left\{ \sum_{m=-M}^{M} \sum_{n=-N}^{N} \left| S_{mn}^y \right|^2 e^{-2\kappa_{mn} y_g} j \frac{k_n}{\kappa_{mn}} R_{mn} \right\} \quad (20)$$

For readability the definitions of the terms shown in (18) - (20) are stated in the Appendix. The forces are a function of velocity (v_x, v_y, v_z) and angular speed ω as well airgap, y_g. For clarify these force dependent terms are not shown in (18) - (20). Due to the assumption that the axial and translational track length is infinitely long and wide the force is not dependent on the x- or z-axis position. Consequently, the stiffness terms in these directions are zero:

$$k_{xx} = k_{yx} = k_{zx} = k_{xz} = k_{yz} = k_{zz} = 0 \quad (21)$$

In contrast, if the method shown in (16) is used to compute the stiffness then a non-zero stiffness will be incorrectly shown to exist along the x-z axis planes [3, 8]. Given (21) the stiffness matrix then considerably simplifies down to

$$[\bar{\mathbf{k}}] = \begin{bmatrix} k_{xx} & k_{xy} & k_{xz} \\ k_{yx} & k_{yy} & k_{yz} \\ k_{zx} & k_{zy} & k_{zz} \end{bmatrix} = -\begin{bmatrix} 0 & \partial F_x / \partial y & 0 \\ 0 & \partial F_y / \partial y & 0 \\ 0 & \partial F_z / \partial y & 0 \end{bmatrix} \quad (22)$$

The height stiffness terms can be determined by substituting the appropriate force term into (22) this yields

$$k_{xy} = -\frac{2wl}{\mu_0} \text{Im} \left\{ \sum_{m=-M}^{M} \sum_{n=-N}^{N} \left| S_{mn}^y \right|^2 e^{-2\kappa_{mn} y_g} R_{mn} \xi_m \right\} \quad (23)$$

$$k_{yy} = -\frac{2wl}{\mu_0} \text{Re} \left\{ \sum_{m=-M}^{M} \sum_{n=-N}^{N} \left| S_{mn}^y \right|^2 e^{-2\kappa_{mn} y_g} R_{mn} \kappa_{mn} \right\} \quad (24)$$

$$k_{zy} = -\frac{2wl}{\mu_0} \text{Im} \left\{ \sum_{m=-M}^{M} \sum_{n=-N}^{N} \left| S_{mn}^y \right|^2 e^{-2\kappa_{mn} y_g} R_{mn} k_n \right\} \quad (25)$$

A. Linearized Force Model

Utilizing the stiffness definition given by (22) a linearized description of the thrust force F_x lift force F_y and lateral force F_z on one EDW rotor can be described by:

$$\begin{bmatrix} F_x \\ F_y \\ F_z \end{bmatrix} \approx \begin{bmatrix} F_{x,s} \\ F_{y,s} \\ F_{z,s} \end{bmatrix} - \begin{bmatrix} k_{xy} \\ k_{yy} \\ k_{zy} \end{bmatrix} \delta_y + [\bar{\mathbf{d}}] \begin{bmatrix} \delta v_x \\ \delta v_y \\ \delta v_z \end{bmatrix} \quad (26)$$

where $[\bar{\mathbf{d}}]$ is the damping matrix [8], and the steady-state force terms are given in (18) - (20). The delta terms in (26) define a small deviation from an equilibrium point. For example:

$$\delta_y = y - y_e \quad (27)$$

$$\delta v_y = v_y - v_{y,e} \quad (28)$$

is an the incremental height change and heave velocity change respectively from equilibrium. The equilibrium value is denoted with the subscript e. It should be noted that the stiffness and damping terms are function of velocity, angular speed and airgap height. But for equation clarity their dependence on these changes are not shown in the coefficient terms. The damping terms are unchanged from what was previously reported in [8] for a conductive sheet flat track.

B. Stiffness Analysis

Using the parameter shown in Table I a surface plot of the calculated lift force as a function of slip s and translational velocity v_x is shown in Fig. 3 for the case when $(v_y, v_z) = (0,0)$. The slip is defined as $s = \omega r_o - v_x$. Fig. 3 shows that the lift force is less dependent on slip at high velocity. The slip provides a means of controlling the thrust/braking magnitude [6]. Using the Table I parameters, the computed stiffness change with slip and velocity is shown in Fig. 4 for the k_{xy} and k_{yy} stiffness terms, respectively. Note that the k_{xz} term is zero when $v_z = 0$ as $F_z = 0$. If a lateral velocity is created through a disturbance, for example if $(v_y, v_z) = (0, 5)$ m/s, then the lateral force F_z will no longer be zero. For this example case, the lateral force F_z and stiffness k_{zy} will have the values as illustrated in Fig. 5. Fig. 5 shows that when the lateral velocity became non-zero, then the EDW will experience lateral instabilty, causing the EDW to drift sideways.
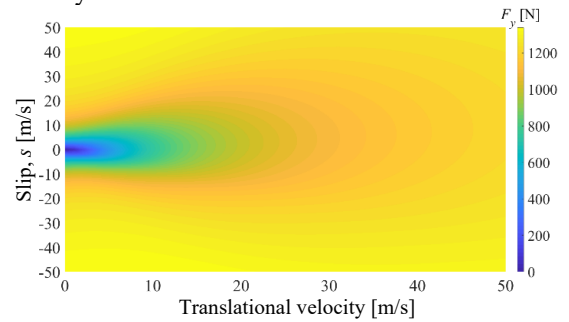

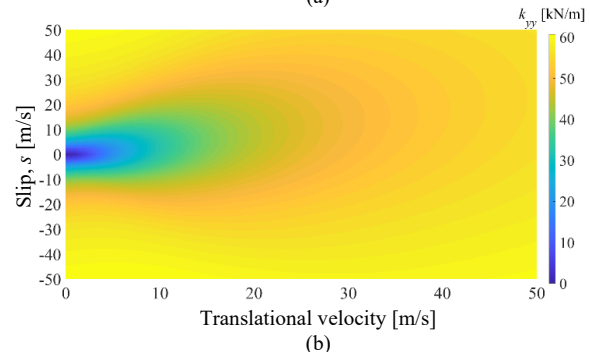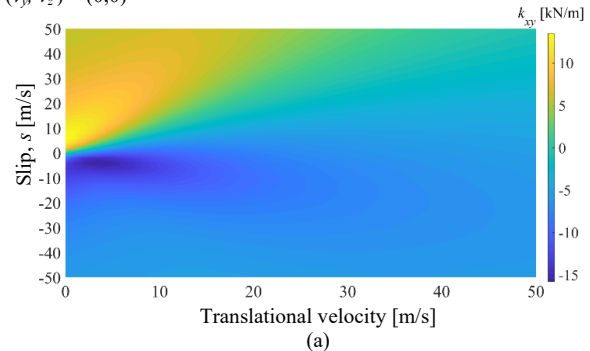Fig. 3. Lift force vs. slip and translational speed for the case when $y_g = 10$ mm and $(v_y, v_z) = (0,0)$

(a)

(b)

Fig. 4. (a) Stiffness surface plot as a function of slip and translational velocity for k_{xy} and (b) k_{yy} when $(v_y, v_z) = (0,0)$ m/s.

III. Model Confirmation

To confirm the model assumptions, two example FEA simulations were performed. In the first a COMSOL 2-D transient FEA simulation was completed in which a single rotor EDW was oscillated back-and-forth in the translational x-axis

whilst maintaining a constant average velocity of $v_x = 50$m/s. The 2-D model neglects the axial rotor edge-effects but does not change the conclusions with respect to the lateral motion. In the second, a JMAG 3-D FEA model was simulated in which there was an oscillating x-axis position centered at $v_x = 0$ m/s.
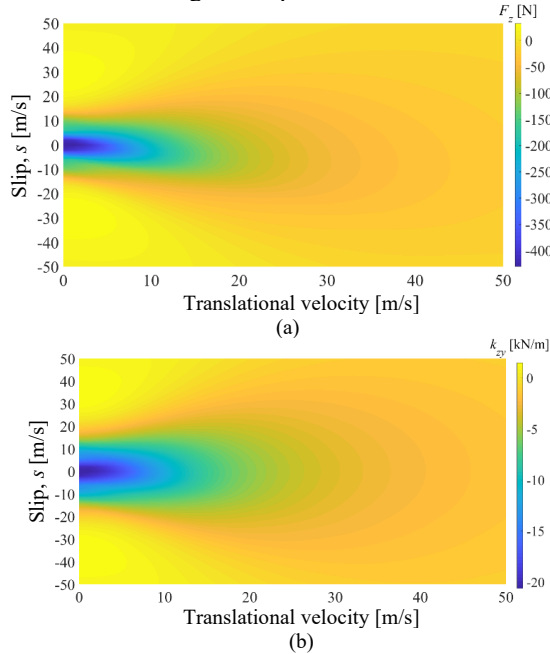

(a)

(b)

Fig. 5. (a) Lateral force F_z and (b) lateral heave stiffness k_{zy} as a function of slip and translational speed for the case when $y_g = 10$ mm and $(v_y, v_z) = (0,5)$

TABLE I. SIMULATION PARAMETERS

Parameter		Value	Units
Rotor	Pole-pairs, P	1	-
	Outer radius, r_o	100	mm
	Inner radius, r_i	25	mm
	Width, $2 \times r_o$	200	mm
	Residual flux density	1.42	T
	Magnet relative permeability	1.055	-
	Air-gap, y_g	10	mm
	Mechanical angular speed, ω	6000	r/min
Track	Thickness, h	12.7	mm
	Conductivity, σ (Cu)	5.69×10^7	S/m
Numerical	Track length, l	20	m
	Track width, w	0.4	m
	Summation indices (M, N)	(2048,128)	-

A. Oscillation Around a Constant Velocity

The 2-D COMSOL model used to simulate a lateral oscillating position is shown in Fig. 1 and the model simulation parameters are shown in Table I. The EDW motion was modelled by:

$$v_x(t) = 50 + 10\sin(\omega_o t) \qquad (29)$$

and $(v_x, v_y) = 0$. The lateral oscillation frequency was choosen to be $\omega_o = 32\pi$ rad/s which is significantly smaller than the rotor angular frequency, which is $\omega = 6000$ rad/s. Fig. 5 shows the simulation comparison. The oscillations using (29) were started at time $t = 0.125$ s. The forces were analytically computed by

$$F_y(v_x) \approx F_{y,s}(v_x) + d_{yx}(v_x)\delta v_x + k_{yx}\delta x \qquad (30)$$

$$F_x(v_x) \approx F_{x,s}(v_x) + d_{xx}(v_x)\delta v_x + k_{xx}\delta x \qquad (31)$$

where δx and δv_x were computed from the change in value between each time-step in the corresponding FEA simulation. The force and damping terms in (30) and (31) are shown as functions of translational velocity. The airgap was assumed fixed.

The normalized lift and thrust forces were evaluated when the stiffness terms $k_{yx} = 0$ and $k_{xx} = 0$. Since the 2-D COMSOL FEA model neglected the source field edge-effects and circulating current the force values for both models were divided by the average of the force. The normalized lift force matched very well, and the thrust force change had a 10% error. The models demonstrate good agreement showing that the k_{yx} and k_{xx} stiffness terms were not needed.
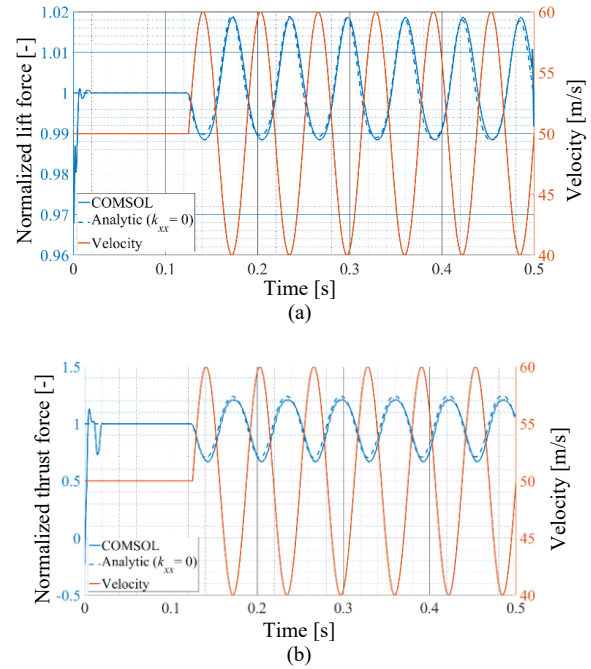

(a)

(b)

Fig. 6(a) Normalized lift force, and (b) normalized thrust force as a function of velocity and time.

B. Oscillation Around Zero Velocity

The 3-D transient magnetic vector potential FEA eddy current solver by JMAG was used to further study the forces created by the rotating EDW that was also translationally oscillating. The JMAG solver cannot model both constant velocity and EDW rotation. Therefore, the velocity oscillation used:

$$v_x(t) = 10\sin(\omega_o t) \qquad (32)$$

where there is no average velocity. The model simulation parameters as shown in Table I were used, except that the rotor radii were reduced to $(r_o, r_i) = (40,10)$ mm so that the simulation size would be lowered. Fig. 7(a) and Fig. 7(b) show the lift and thrust force comparsion between the analytic and FEA model. The analytic force results are shown for the case when (30) and (31) are used with all stiffness terms non-zero, and also for the case when $k_{yx} = 0$ and $k_{xx} = 0$ are zero. The large error caused by the inclusion of the added stiffness terms is self-evident.

CONCLUSION

This paper has demonstrated through an equation derivation and through transient FEA simulations that the translational and lateral stiffness terms, such as k_{xx}, k_{zz} and cross coupling terms such as $k_{yx}, k_{yz}, k_{zx}, k_{xz}$ for an infinitely wide uniform conductive track are zero. This analysis corrects prior work that derived incorrect non-zero stiffness terms in these axes. The paper also

highlights how the cross-coupling stiffness term k_{zy} creates lateral instability even with an infinite-wide track assumption.
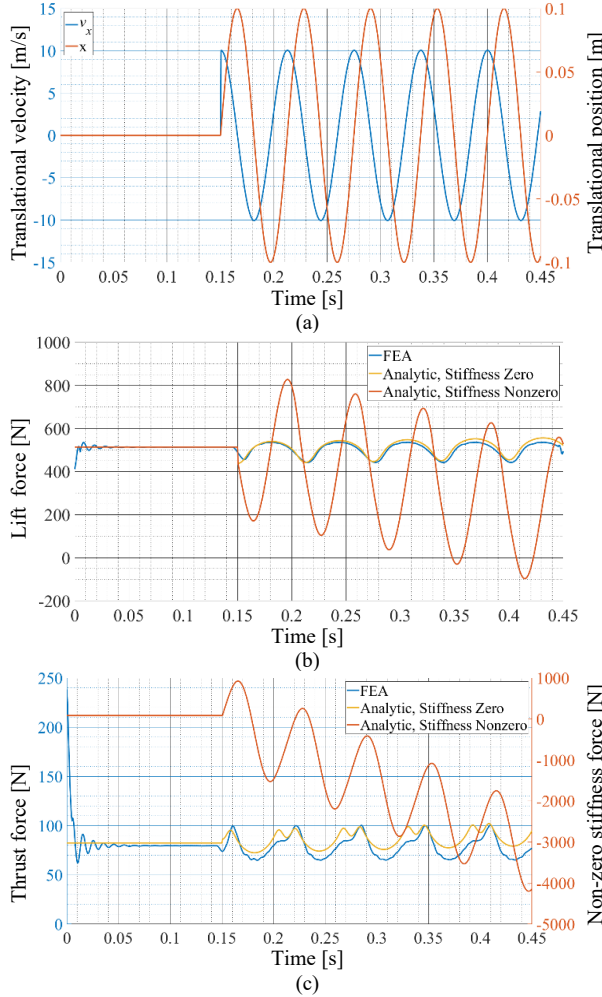

Fig. 7.(a) Translational velocity and translational position, (b) lift force and (c) Thrust force as a function of time. When including the incorrect stiffness terms the thrust force is a factor of ~10× higher than it should be, indicating the magnitude of error if including the incorrect translational stiffness terms.

APPENDIX

The force terms defined in (18)- (20) were derived in [6]. The reflection term, R_{mn}, is defined by:

$$R_{mn} = \frac{\mu_0 \sigma \tau_{mn}}{\kappa_{mn}^2 + \gamma_{mn}^2 + 2\kappa_{mn}\beta_{mn}\coth(\beta_{mn}h)} \quad (33)$$

$$\kappa_{mn}^2 = \xi_m^2 + k_n^2 \quad (34)$$

$$\xi_m = 2\pi m / l \quad (35)$$

$$k_n = 2\pi n / w \quad (36)$$

$$\beta_{mn}^2 = \lambda^2 + \gamma_{mn}^2 \quad (37)$$

$$\lambda = -0.5 v_y \mu_0 \sigma \quad (38)$$

$$\gamma_{mn}^2 = \kappa_{mn}^2 - j\mu_0\sigma\left(P\omega + \xi_m v_x + k_n v_z\right) \quad (39)$$

$$\tau_{mn} = \kappa_{mn} v_y + j\left(P\omega + \xi_m v_x + k_n v_z\right) \quad (40)$$

Table I defines the variables. The source field term in (18)- (20) is determined by evaluating [7, 8]

$$S_{mn} = \frac{1}{lw} \int_{-w/2}^{w/2} \int_{-l/2}^{l/2} B_y^{so}(x, y_g, z, t) e^{-j\xi_m x} e^{-jk_n z} dx dz \quad (41)$$

where the source field term in (41) is modeled by evaluating:

$$B_y^{so}(x, y, z, t) =$$

$$\frac{B_r r_o e^{-jP\omega t}}{2\pi} \int_0^{2\pi} \int_{-w_o/2}^{w_o/2} \frac{e^{jP\theta_o}}{R^3}(y - y_c - r_o \sin\theta_o) dz_o d\theta_o \quad (42)$$

where

$$R = [(x - x_c - r_o\cos\theta_o)^2 + (y - y_c - r_o\sin\theta_o)^2 + (z - z_c - z_o)^2]^{1/2} \quad (43)$$

The Halbach rotor origin is located at $(x_c, y_c, z_c) = (0, r_o + y_g, 0)$. With $P=1$, the radial flux density magnitude term is

$$B_r = B_{res} \frac{(1 + \mu_r)(r_i^2 - r_o^2)}{[(1 - \mu_r)^2 r_i^2 - (1 + \mu_r)^2 r_o^2]} \quad (44)$$

where B_{res} = residual flux density, μ_r = magnet relative permeability. The integration of (42) with respect to z_o was performed analytically whereas the integration with respect to θ_o was numerically evaluated.

REFERENCES

[1] P. Lin, Z. Deng, Z. Ke, W. Lei, X. Wang, and K. Ren, "Dynamic Characteristics and Working Modes of Permanent Magnet Electrodynamic Suspension Vehicle System Based on Six Wheels of Annular Halbach Structure," *Technologies,* vol. 11, no. 1, p. 16, 2023.

[2] H. Shi *et al.*, "An Effective Optimization Method and Implementation of Permanent Magnet Electrodynamic Wheel for Maglev Car," *IEEE Transactions on Vehicular Technology,* pp. 1-13, 2023.

[3] J. Wright and J. Z. Bird, "Analytic damping and stiffness analysis for a 4-DOF electrodynamic wheel maglev vehicle," in *2018 XIII Intern. Conf. Elect. Mach.* , 2018, pp. 555-561.

[4] C. Bruce *et al.*, "An Electrodynamic Wheel Maglev Vehicle with a Passive U-Guideway," in *Intern. Conf. Elect. Mach. Sys.*, Chiang Mai, Thailand, Nov. 29 - Dec. 2 2022.

[5] W. Qin, M. Yuhua, L. Gang, W. Fuyao, S. Chengrui, and Z. Jielong, "Investigation of Asymmetric Axial-flux Hybrid Excited Electrodynamic Wheels for Maglev Transportation," in *2021 IEEE Energy Conv. Cong. Expo. (ECCE)*, 10-14 Oct. 2021, pp. 3753-3758.

[6] S. Paul, "Three-dimensional steady state and transient eddy current modeling," Ph.D. Thesis, Elect. Comp. Eng., Univ. N.C. at Charlotte, Charlotte,NC, 2014.

[7] S. Paul, W. Bomela, N. Paudel, and J. Z. Bird, "3-D Eddy Current Torque Modeling," *IEEE Trans. Mag.,* vol. 50, no. 2, pp. 905-908, 2014.

[8] S. Paul, J. Wright, and J. Z. Bird, "3-D Steady-State Eddy-Current Damping and Stiffness Terms for a Finite Thickness Conductive Plate," *IEEE Trans Magn.,* vol. 50, no. 11, pp. 1-4, 2014.

[9] T. Theodoulidis and J. R. Bowler, "Interaction of an eddy-current coil with a right-angle conductive wedge," *IEEE Trans. on Mag.,* vol. 46, no. 4, pp. 1034-1042, 2010.

[10] A. Musolino, R. Rizzo, and E. Tripodi, "Travelling Wave Multipole Field Electromagnetic Launcher: An SOVP Analytical Model," *IEEE Transactions on Plasma Science,* vol. 41, no. 5, pp. 1201-1208, 2013.

[11] Y. Chen, W. Zhang, J. Z. Bird, P. Subhra, and K. Zhang, "A 3-D Analytic Based Model of a Null-Flux Permanent Magnet Halbach Array Electrodynamic Suspension Device," *IEEE Trans. Magn.,* vol. 51, no. 11, pp. 1-5, Nov. 2015, Art no. 8300405.

[12] O. D. Jefimenko, *Electricity and Magnetism*. New York: Meredith Publishing Co., 1966.

[13] E. P. Furlani, *Permanent magnet and electromechnaical devices materials, analysis, and applications*. San Diego: Academic Press, 2001.

[14] E. P. Furlani, S. Reznik, and W. Janson, "A three-dimensional field solution for bipolar cylinders," *IEEE Trans. Magn.,* vol. 30, no. 5, pp. 2916-2919, 1994.